Available online at www.sciencedirect.com
ScienceDirect
Journal of Nuclear Materials 374 (2008) 313–319
journal of nuclear materials
www.elsevier.com/locate/jnucmat

Adiabatic shearing behavior of different steels under extreme high shear loading

Woei-Shyan Lee *, Chen-Yang Liu, Tao-Hsing Chen

Department of Mechanical Engineering, National Cheng Kung University, Tainan 701, Taiwan

Received 28 April 2007; accepted 6 September 2007

Abstract

The adiabatic shearing behavior of S15C low carbon steel, S50C medium carbon steel, and SKS 93 tool steel with a high carbon and low alloy content (abbreviated to high carbon steel hereafter) is examined using a compressive-type split-Hopkinson pressure bar (SHPB) at strain rates ranging from $(5–20)\times10^4\ s^{-1}$. Metallographic observations of the sheared specimens suggest that the shear flow stress and the hardness and width of the shear band depend strongly on the carbon content and strain rate. The formation of the deformed and martensitic transformed shear bands is a function of the carbon content and the shear load. The fracture surface of the low carbon steel exhibits a dimple-like structure. However, the fracture surfaces of the medium and high carbon steels exhibit both a dimple-like structure and knobby features. The formation of the knobby features is attributed to an increased carbon content and a higher strain rate.
© 2007 Elsevier B.V. All rights reserved.

PACS: 62.20.Fe; 81.70.Bt; 81.05.Bx; 81.40.Np

1. Introduction

Carbon steel plays an important and enduring role among commercially available materials because of its excellent ductility, wide range of selectable mechanical properties following heat treatment and comparatively low cost [1,2]. Carbon steel is widely applied for a diverse range of applications within a variety of different fields, including the structural elements, the automotive industry and the nuclear power plants, for example [3]. Typical applications in nuclear power plants include the reactor, the cooling water system, metallic containers and piping systems. Furthermore, spent nuclear fuel is generally transported within carbon steel casks. These casks may become damaged as a result of mishandling or accidents, leading to a reduction in their mechanical integrity. Droste et al. [4] investigated an extreme case in which a spent fuel cask was exposed to the explosive effects of an LPG tank ruptured by fire. The results showed that the explosive event was accompanied by an expanding fire ball, heat radiation, and an intense pressure, which not only projected fragments of the ruptured tank toward the cask, but also moved the cask 7 m from its original position. While a post-test inspection revealed that the cask remained leak tight and maintained its mechanical integrity, it is nevertheless vital that the dynamic flow response and adiabatic shear banding behavior of carbon steels are well understood such that the safety of all carbon steel components used throughout the nuclear power industry can be similarly assured.

The term 'adiabatic shearing' was first coined by Zener and Hollomon [5] in 1944. The authors proposed that if the strength loss caused by thermal softening exceeds the strength increase induced by strain or strain rate hardening, the plastic deformation becomes unstable and gives way to a localized band-like deformation mode, i.e. shear bands. Adiabatic shearing is an important phenomenon found in many materials deformed at high strain rates. Shear band formation is a complex function of strain, strain rate and temperature. Shear bands have been

* Corresponding author. Tel.: +886 6 2757575x62174; fax: +886 6 2352973.
E-mail address: wslee@mail.ncku.edu.tw (W.-S. Lee).

0022-3115/$ - see front matter © 2007 Elsevier B.V. All rights reserved.
doi:10.1016/j.jnucmat.2007.09.002

observed in many practical applications involving high-speed deformation, including machining, ballistic penetration, and high-speed forming [6,7]. Hence, many investigations into adiabatic shear band formation have been published over the past 20 years or so [8,9]. Since steel is the most widely used of all metals and finds application in a huge number of fields, developing a detailed insight into the formation of adiabatic shear bands in steel materials is highly desirable. Accordingly, the present study uses a compressive-type SHPB apparatus to impact S15C low carbon steel, S50C medium carbon steel and SKS93 high carbon tool steel specimens under strain rates ranging from $(5–20)\times10^4\ s^{-1}$. The behavior and microstructure of the three carbon steels under forced localized shear are examined and compared.

2. Materials and experimental procedure

The carbon steels investigated in the present study were all received in plate form with a thickness of 32 mm. The low carbon and medium carbon steels were supplied by China Steel Corp. (Taiwan), while the high carbon steel was acquired from Daido Steel Corp. (Japan). The chemical compositions of the three carbon steels, as measured by a glow discharge spectrometer (GDS), are summarized in Table 1. The compositions of the three steels satisfy the JIS code for S15C, S50C and SKS93, and are similar to AISI 1015, AISI 1050 carbon steels and AISI W4 tool steel, respectively. In order to alleviate residual stresses and to ensure a uniform microstructure, the as-supplied plates were vacuum-annealed at 820 °C for 2 h and then left to cool in the furnace.

Table 1
Composition of three carbon steel specimens

Element	C	Si	Mn	P	S	Cu	Ni	Cr	Fe
S15C	0.15	0.26	0.79	0.02	0.01	0.04	0.03	0.02	Bal.
S50C	0.48	0.22	0.77	0.019	0.02	0.01	0.03	0.01	Bal.
SKS93	1.16	0.25	0.80	0.01	0.003	0.03	0.032	0.32	Bal.

The current hat-shaped specimens, first introduced by Hartmann et al. [10], were machined from the annealed plates with the dimensions shown in Fig. 1(a). As in the compressive SHPB experiment presented in [11] by the current authors, the specimens were sandwiched between the incident and transmitted bars of the SHPB apparatus, as shown in Fig. 1(b). The geometry of the hat-shaped specimens was such that the compressive stress wave produced by the impact of the incident bar generated an adiabatic shear deformation, localized within a narrow region of the test piece. To prevent the rim part of the specimen from assuming a barrel-like shape during impact testing, thereby influencing the accuracy of the shear band width measure-

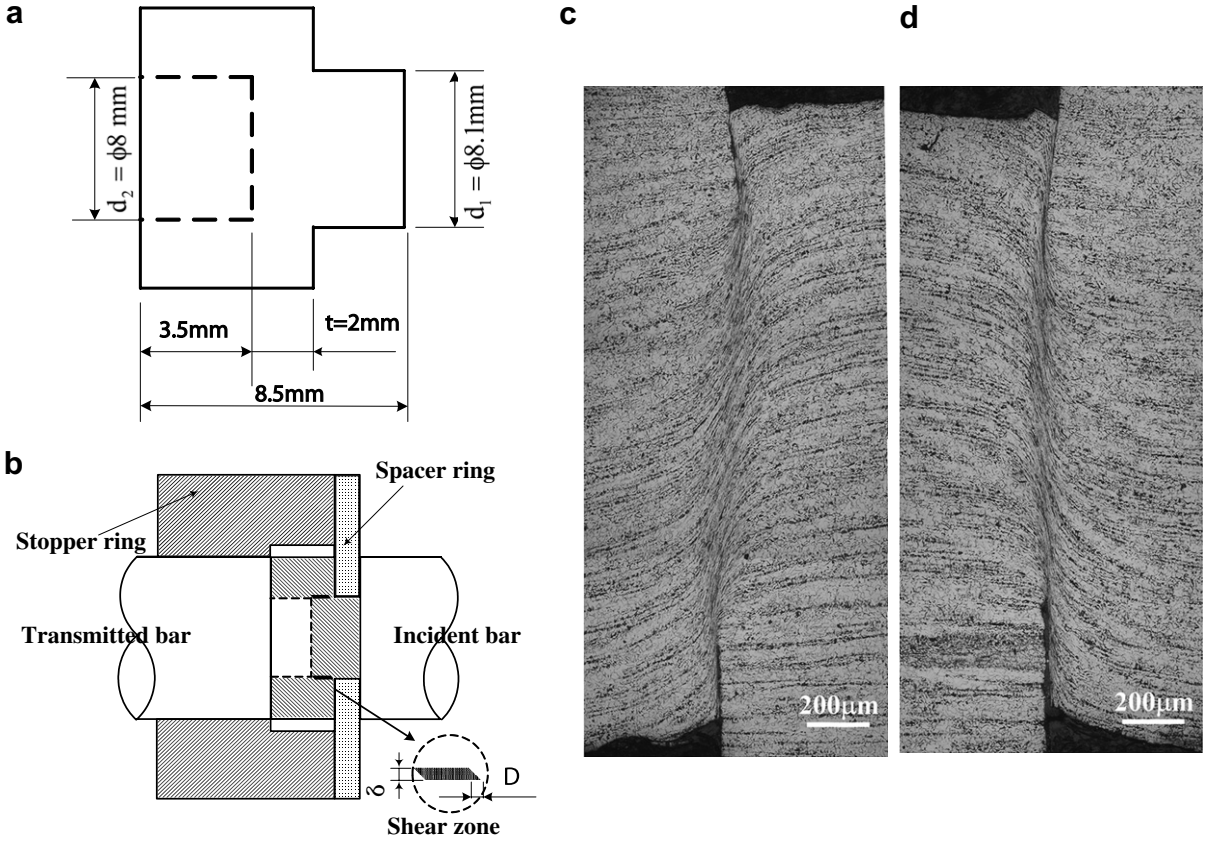

Fig. 1. (a) Dimensions of specimens; (b) Modified experimental setup. Optical micrographs of shear zone in S15C steel specimens under strain rates of: (c) $5.0\times10^4\ s^{-1}$ and (d) $2.0\times10^5\ s^{-1}$.

ment, a stopper ring was fitted around the head of the SHPB transmitted bar and the specimen, as shown in Fig. 1(b). The stopper ring was fixed to the transmitted bar at the desired position using a pressure screw. The shear stress (τ) and compression displacement (D) were determined from the reflected wave ε_r and the transmitted ε_t wave in accordance with $\tau = 2EA\varepsilon_t[\pi(d_1 + d_2)t]^{-1}$ and $D = -2C_0 \int \varepsilon_r \, dt$, respectively, where A, E and C_0 are the cross-sectional area of the incident and transmitted bars, Young's modulus and sonic wave speed of the pressure bars, respectively, and d_1, d_2 and t are the external diameter, internal diameter and shear zone thickness of the specimen, respectively. The nominal shear strain (γ) and nominal strain rate ($\dot{\gamma}$) were defined as $\gamma = D/\delta$ and $\dot{\gamma} = \partial\gamma/\partial t$, respectively, where δ is the width of the shear band as measured using an optical microscope. The relationship between D and δ is presented in Fig. 1(b). According to the strain rate definition given above, the strain rate varies as a function of time and therefore induces a gradual change in the specimen microstructure over the course of the deformation process, as reported by Ryazanov et al. [12]. In the current tests, the specimens were deformed at strain rates of $5 \times 10^4\ s^{-1}$, $1.0 \times 10^5\ s^{-1}$ and $2.0 \times 10^5\ s^{-1}$, respectively, under a fixed displacement of $D = 0.7$ mm, resulting in the formation of shear bands in the shear zones. As shown in Fig. 1(c) and (d), specimen fracture (i.e. cracking) is constrained to the region immediately ahead of the tail ends of the adiabatic shear bands. Microstructural observations of the deformed specimens were carried out using an Axiovert 200MAT optical microscope. Meanwhile, the fracture surfaces were examined using a JEOL JSM840 scanning electron microscope (SEM) operated at 15 kV.

3. Results and discussion

3.1. Mechanical response

Fig. 2(a) presents the stress–displacement curves of the S15C, S50C and SKS93 steels under strain rates of $5.0 \times 10^4\ s^{-1}$ and $2.0 \times 10^5\ s^{-1}$, respectively. The curves show that each steel is work softened after it initially yields, but subsequently work hardens until a stress drop is induced by adiabatic heating. The abrupt increase in stress observed at the final stage of the deformation process is caused by the impact of the incident bar on the spacer ring. It is apparent that the flow stress of each steel increases with increasing strain rate. Moreover, it can be seen that an increased carbon content leads to a more significant strengthening effect during the dynamic shearing deformation process. Regarding the increased shear stress induced at higher strain rates, it is found that the steel with a higher carbon content is more sensitive to the strain rate. This result is similar to that reported by the current group for the behavior of the same steels under dynamic impact deformation [10]. The average temperature rise within the shear band can be estimated by the function $\Delta T = (\rho C)^{-1} \int \tau \, d\gamma$, where ρ is the density of steel ($7.83\ kg/m^3$) and C is the specific heat (0.49 kJ/kg/°C). Fig. 2(b) plots ΔT as a function of the nominal shear strain for the three tested steels. According to the present experimental data, the duration of the deformation process is less than 100 μs. Therefore, the deformation of the steel within the shear band generates a huge temperature rise over a very short period of time. From Fig. 2(b), it can be seen that ΔT increases with increasing carbon content, strain rate and strain.

3.2. Optical microstructural (OM) observation

Table 2 summarizes the width and average hardness of the shear bands formed in the three specimens under each of the loading conditions. Note that the width of the shear band is defined as the width of the high viscous flow region,

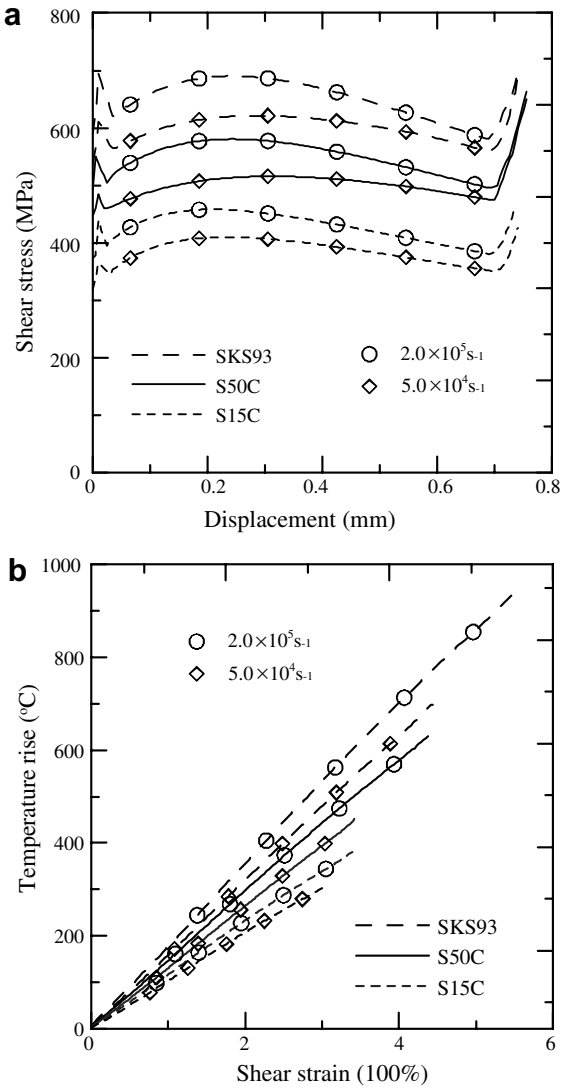

Fig. 2. (a) Stress–displacement curves of three carbon steels under strain rates of $5.0 \times 10^4\ s^{-1}$ and $2.0 \times 10^5\ s^{-1}$, respectively; (b) calculated average temperature rise within shear band.

Table 2
Width and average hardness of shear bands in three steel specimens

Steels	5.0×10^4 s^{-1}		1.0×10^5 s^{-1}		2.0×10^5 s^{-1}	
	Width (μm)	Hardness (Hv)	Width (μm)	Hardness (Hv)	Width (μm)	Hardness (Hv)
S15C	242	265	213	271	218	287
S50C	219	310	196	330	169	356
SKS93	171	351	154	376	134	405

i.e. the region in which the shear flow slip lines and grain distortion are clearly evident compared to the matrix microstructure. Furthermore, the average hardness data denote the mean hardness values obtained from ten separate hardness tests performed within the cross-sectional shear band region. It is observed that the bandwidth decreases with an increasing carbon content and strain rate, whereas the average hardness increases. The optical micrographs presented in Fig. 3(a) and (b) show that the shear bands formed in the S15C and S50C specimens at a strain rate of 1.0×10^5 s^{-1} are broadly similar. However, the microstructure of the shear band formed in the SKS93 steel specimen at the same strain rate is markedly different (see Fig. 3(c)). Specifically, the shear flow slip lines are not so well developed, and the higher carbon content results in a proliferation of microcracks and micropores, which grow and coalescence, prompting a higher degree of cracking. Comparing the shear band morphologies of the three carbon steels shown in Fig. 3, it is seen that the S50C and SKS93 specimens contain both deformed and martensitic transformed bands, while the S15C specimen has only a deformed band. In Fig. 3(a), the elongation and distortion of the ferrite grains in the S15C specimen become more pronounced towards the center of the shear band. The distortion angle (θ), defined and plotted on the micrograph, increases from 40° to 84° as the measurement point is shifted from B to A. A similar phenomenon is also found in the S50C and SKS93 specimens, as shown in Fig. 3(b) and (c), respectively. These results indicate that the distortion angle of the three carbon steels increases with decreasing distance from the center of the shear band. In other words, the deformation within the shear band is inhomogeneous. The local shear strain (γ) can be defined as $\gamma = \tan\theta$ [13]. Applying this definition, the maximum local strain, which occurs near the center of the transformed band, of the S50C and SKS93 steel specimens is found to exceed 70. Similarly, the maximum local shear strain in the S15C specimen, located in the center of the deformed band, is approximately 10. The maximum local shear strain, γ, of these three steels is much higher than the nominal strain shown in Fig. 2(b). Therefore, the actual

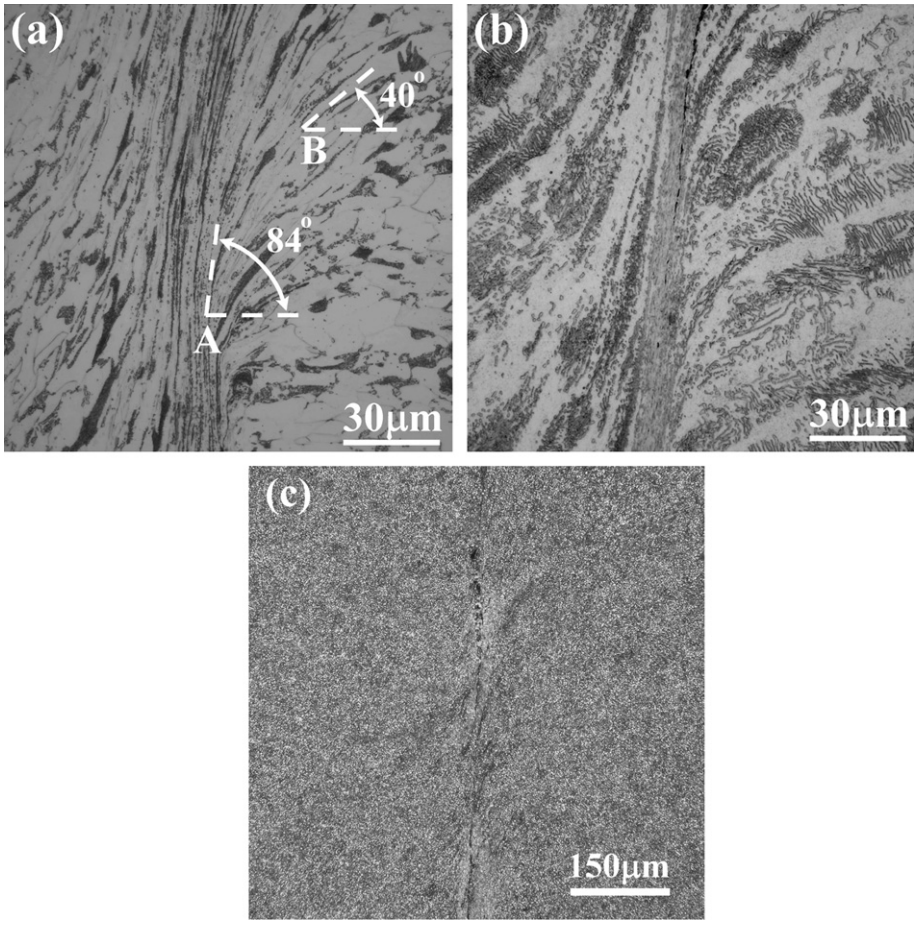

Fig. 3. Micrographs of adiabatic shear bands in: (a) S15C, (b) S50C and (c) SKS93 steel specimens under strain rate of 1.0×10^5 s^{-1}.

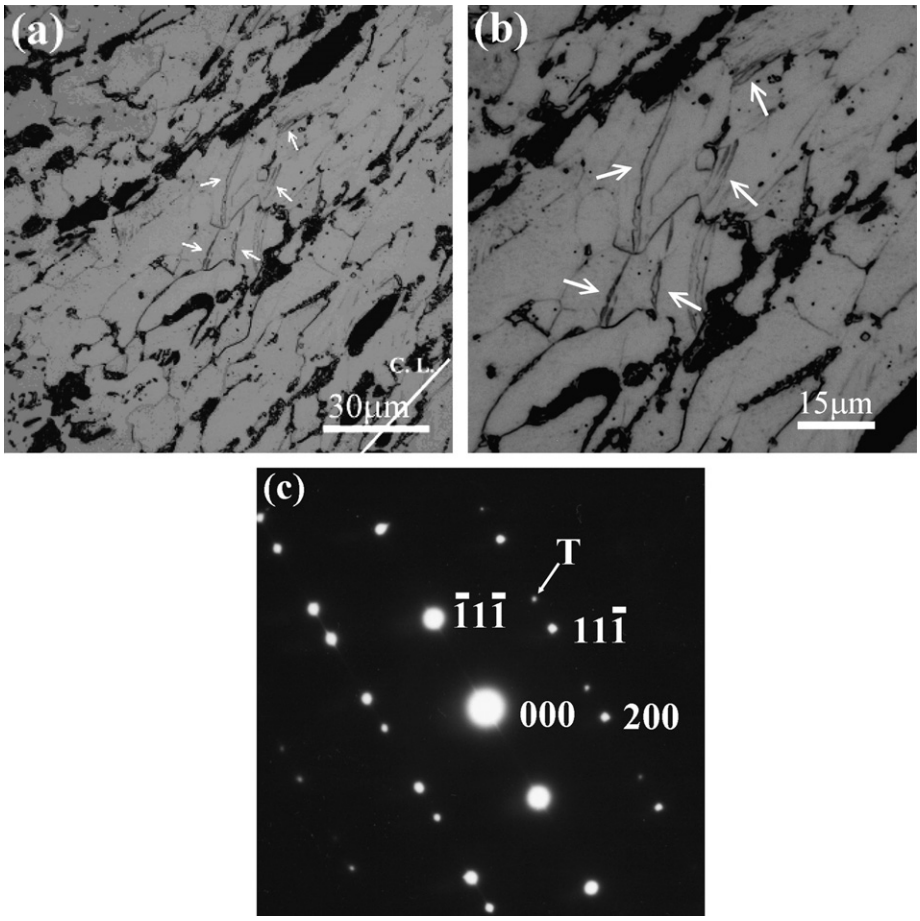

Fig. 4. (a) Micrograph of mechanical twins in S15C specimen under strain rate of $2.0 \times 10^5\ s^{-1}$; (b) high-magnification view of specimen shown in (a); (c) TEM diffraction pattern of twins shown in (a).

temperature rise in these areas may be higher than that indicated by ΔT. Regarding the distribution of the local strain within the shear band, it can be concluded that the shear deformation model for the S15C, S50C and SKS93 steels considered in this study is consistent with the softening model proposed by Lamouroux et al. [14], which also considers high strain rate deformation. Mechanical twins are observed in the S15C low carbon steel specimen sheared at a strain rate of $2.0 \times 10^5\ s^{-1}$, as shown in Fig. 4. In Fig. 4(a) several twins (indicated by the arrows) are evident; located at approximately 60 μm from the center of the shear band. Fig. 4(b) presents a high-magnification view, while Fig. 4(c) shows the TEM diffraction pattern of the twins (T) shown in Fig. 4(a). It is known that a small grain size limits the development of twins [15]. The ferrite grain sizes of low carbon steel, medium carbon steel and high carbon steel are approximately 35 μm, 25 μm and 18 μm, respectively. Thus, twins are found only in the S15C low carbon steel specimens.

3.3. Fractographs

The fracture of the present specimens is dominated by localized shearing. In each case, cracks propagate along the central region of the adiabatic shear band. Fig. 5(a) and (b) present fractographs of the S15C steel specimen deformed at strain rates of $5.0 \times 10^4\ s^{-1}$ and $2.0 \times 10^5\ s^{-1}$, respectively. The presence of elongated dimples on the fracture surfaces is clearly observed. The small cavities visible in Fig. 5(b) are micropores formed during the adiabatic heating and softening of the specimen under extremely high shear loading conditions. Comparing Fig. 5(a) and (b), it is seen that the depth of the dimples increases with increasing strain rate, which suggests that the temperature in the adiabatic shear band formed under a high strain rate is higher than that in the band formed under a low strain rate. In other words, the specimen deformed at a strain rate of $2.0 \times 10^5\ s^{-1}$ exhibits a more ductile behavior under fracture. In Fig. 5(c) and (d), which show the fracture morphologies of S50C medium carbon steel, it is seen that the two fracture surfaces not only have a dimple-like structure but also contain knobby features. Furthermore, it is clear that the size of the knobby region increases with increasing strain rate. Comparing the fractographs of the S15C and S50C specimens, two obvious differences are observed, namely the appearance of knobby features in the latter and a smaller dimple size on the S50C fracture surface than on the S15C surface. This indicates that the deformation

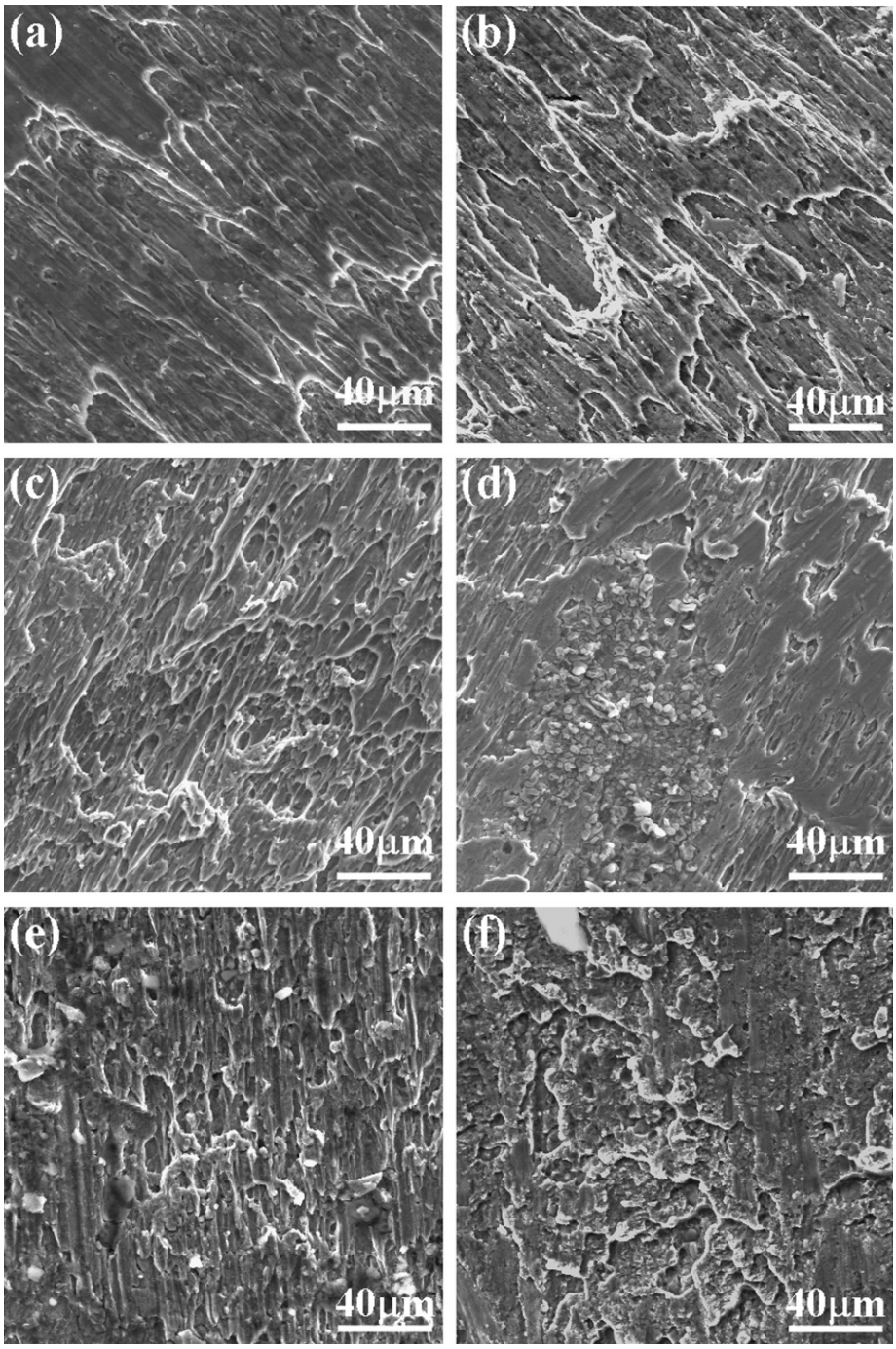

Fig. 5. Fracture morphologies of: (a) S15C steel deformed under $5.0 \times 10^4\ s^{-1}$; (b) S15C steel deformed under $2.0 \times 10^5\ s^{-1}$; (c) S50C steel deformed under $5.0 \times 10^4\ s^{-1}$; (d) S50C steel deformed under $2.0 \times 10^5\ s^{-1}$; (e) SKS93 steel deformed under $5.0 \times 10^4\ s^{-1}$; and (f) SKS93 steel deformed under $2.0 \times 10^5\ s^{-1}$.

resistance of medium carbon steel in the shear band is greater than that of low carbon steel. This finding is consistent with the flow behaviors shown in Fig. 2(a). Fig. 5(e) and (f) present fractographs of the SKS93 steel fracture surface at strain rates of $5.0 \times 10^4\ s^{-1}$ and $2.0 \times 10^5\ s^{-1}$, respectively. As in the S50C specimen, the fracture surface contains both knobby features and dimples. As before, it is noted that the size of the knobby feature area increases with increasing strain rate. Compared to the S50C fracture surface, the knobby area on the SKS93 fracture surface is larger, and the dimples are slightly smaller.

4. Conclusions

Using hat-shaped specimens, this study has shown that the shear stress and hardness of S15C low carbon steel, S50C medium carbon steel and SKS93 high carbon steel increase with an increasing carbon content and strain rate.

The average temperature rise within the shear bands formed within the various specimens has been calculated and has been shown to increase with increasing strain rate and carbon content. Conversely, the widths of the shear bands decrease with increasing strain rate and carbon content. Both deformed and martensitic transformed shear bands have been found in the S50C and SKS93 steel specimens. However, only deformed shear bands have been observed in the S15C low carbon steel. The local shear strain is inhomogeneous within the shear band of each steel. The maximum localized strain of 70, found near the transformed band, for the S50C and SKS93 specimens is much higher than that of 10, located near the center of the shear band, for the S15C steel specimen. The fracture surfaces of the medium and high carbon steels contain both knobby features and dimples. The size of the knobby area increases with strain rate and carbon content. By contrast, the fracture surface of the low carbon steel specimen contains only dimples. These results suggest that the temperature rise in the shear bands of the S50C and SKS93 steels is higher than that in the S15C specimen. Although transformed bands have been identified in the S50C and SKS93 steel specimens, no cleavage fracture characteristics have been found on the fracture surfaces of any of the present steels. Therefore, it can be inferred that these carbon steels have an excellent shear deformation resistance.

Acknowledgements

The current authors gratefully acknowledge the financial support provided to this study by the National Science Council (NSC) of Taiwan under Grant No. NSC 94-2212-E-006-038.

References

[1] S. Kalpakjian, Manufacturing Processes for Engineering Materials, Addison Wesely Longman, CA, 1997, p. 122.
[2] B.J. Hogan, Manuf. Eng. 120 (1998) 42.
[3] D.J. Antos, E.G. Nisbett, in: E.G. Nisbett, A.S. Melilli, (Eds.), Steel Forgings: Second Volume, USA, ASTM Committee A-1, p. 129.
[4] B. Droste, U. Probst, W. Heller, RAMTRANS 10 (4) (1999) 231.
[5] C. Zener, J.H. Hollomon, J. Appl. Phys. 15 (1944) 22.
[6] J.Q. Xie, A.E. Bayoumi, H.M. Zbib, Int. J. Mach. Tools Man. 36 (1944) 835.
[7] S.N. Dikshit, V.V. Kutumbarao, G. Sundararajan, Int. J. Imp. Eng. 16 (1995) 293.
[8] K.M. Cho, S. Lee, S.R. Nutt, J. Duffy, Acta Metall. Mater. 41 (1993) 923.
[9] T. Børvik, M. Langseth, O.S. Hopperstad, K.A. Malo, Int. J. Impact Eng. 27 (2002) 19.
[10] K.H. Hartmann, H.D. Kunze, L.W. Meyer, Metallurgical effects on impact loaded materials, in: M.A. Meyers, L.E. Murr (Eds.), Shock Wave and High-Strain-Rate Phenomena in Metals, 1981, p. 325.
[11] W.S. Lee, C.Y. Liu, Metall. Trans. 36A (2005) 3175.
[12] A.I. Ryazanov, V.V. Dremov, M. Kiritani, Radiat. Eff. Def. Solids 157 (1) (2002) 209.
[13] Y.B. Xu, W.L. Zhong, Y.J. Chen, L.T. Shen, Q. Liu, Y.L. Bai, M.A. Meyers, Mater. Sci. Eng. A 299 (2001) 287.
[14] C. Lamouroux, P. Debat, J. Ingles, N. Guerrero, P. Sirieys, J.C. Soula, Mech. Mater. 18 (1994) 79.
[15] K. Wongwiwat, L.E. Murr, Mater. Sci. Eng. 35 (1978) 273.